

# Chiral Maxwell waves in continuous media from Berry monopoles

M. Marciani and P. Delplace  
*Univ Lyon, Ens de Lyon, Univ Claude Bernard,  
CNRS, Laboratoire de Physique, F-69342 Lyon, France*

The characterization of a bulk-boundary correspondence for continuum systems has proven to be challenging due to the lack of a (compact) Brillouin zone. The macroscopic Maxwell's equations rule the small- $\mathbf{k}$  (small-momenta) behavior of light propagating in a medium. It has been shown that a standard bulk-boundary correspondence can be recovered if the response matrix in the limit  $\mathbf{k} \rightarrow \infty$  obeys a certain regularity. Conversely if one is to deal with atomic crystals, one may give up macroscopic Maxwell's equation and opt for a full but hard-to-get description at all wavelengths in the Brillouin Zone. Here, we propose a radically different approach valid for smooth interfaces. Remarkably, the spectral flows can be predicted without the need of regularity at big  $\mathbf{k}$ . The number of topologically protected modes localized at the contact surface of two materials is computed calculating the Berry flux emanated from bands-degeneracy points in the parameter space of the system.

In the last decades, the inclusion of topological analysis in condensed matter systems has lead to a more comprehensive understanding of their properties<sup>1,2</sup> and inspired applications for a technological advance beyond the realm of quantum electronic systems<sup>3,4</sup>, most notably in classical waves physics such as photonics<sup>5</sup>, mechanics<sup>6-8</sup> or acoustics<sup>9,10</sup>

A remarkable consequence of a non-trivial topology in wave physics is the presence of uni-directional (chiral) eigenmodes that perfectly propagate along interfaces between two materials<sup>11</sup> despite the presence of defects or weak disorder. The key mathematical object to determine the number of such modes in two-dimensional setups is the so-called (first) Chern number. Notably, this quantity can be computed only in systems where the momentum space of the bulk materials is compact, mainly limiting the applicability of this tool to crystals, where the natural base space is the two-dimensional (2D) Brillouin zone that is a torus<sup>12</sup>. As a consequence the topological analysis of chiral waves in well-known continuous models appearing naturally in the context of optics, geophysics, mechanics and fluid mechanics has been put aside for a long time, being introduced only recently<sup>13-17</sup>. Actually, the unbounded momentum space of such models is equivalent to a compact one if the parameters involved in the partial differential equations satisfy certain conditions in the large-momentum limit<sup>18,19</sup>. Though simple and powerful, this approach suffers of being not obviously applicable to real materials, since most continuous approximations inevitably break down in the large momenta limit.

Here we suggest a different and more universal route where the emergence of interface chiral optical waves is predicted from the existence of degeneracy points in parameter space. These points behave as topological charges, or Berry monopoles, whose flux through a close surface surrounding them is also a Chern number. In that sense, the topological origin of interface chiral states is encoded into a local quantity that can be seen as a topological defect in parameter space, and thus does not require any additional regularization at large wavenum-

ber as it is usually done in optical continua<sup>13,14</sup>. This approach is therefore particularly suitable to address topological properties in continuum systems in general, and was recently used to reinterpret<sup>20</sup> and predict<sup>21</sup> topological fluid waves in the geo/astro-physical context. Adapting this method to the realm of electromagnetism in continuous media, we apply the theory to predict the existence of chiral optical waves at the interface between metals, gyro-electric and gyro-magnetic materials.

## Maxwell equations for gyrotropic materials

The macroscopic Maxwell's equations govern the behavior of the macroscopic averages of the electromagnetic fields. They describe the 3+1D dynamics of the four fields  $\mathbf{D}, \mathbf{E}, \mathbf{B}, \mathbf{H}$  under the influence of external sources (the distribution of charges  $\rho$  and the distribution of current  $\mathbf{J}$ ).

$$\nabla \times \mathbf{E} = -\frac{\partial \mathbf{B}}{\partial t} \quad \nabla \times \mathbf{H} = \frac{\partial \mathbf{D}}{\partial t} + \mathbf{J} \quad (1)$$

$$\nabla \cdot \mathbf{D} = \rho \quad \nabla \cdot \mathbf{B} = 0 \quad (2)$$

This set of partial differential equations are complemented by material-dependent constitutive equations relating algebraically the fields. We assume they are of the most general form that accommodates homogeneous and linear responses including magneto-electric effects

$$\begin{pmatrix} \mathbf{D} \\ \mathbf{B} \end{pmatrix} = M \circ \begin{pmatrix} \mathbf{E} \\ \mathbf{H} \end{pmatrix} \quad \text{where } M := \begin{pmatrix} \varepsilon & \xi \\ \zeta & \mu \end{pmatrix}. \quad (3)$$

Here,  $\varepsilon$  and  $\mu$  are respectively the permittivity and permeability  $3 \times 3$  tensors while  $\xi$  and  $\zeta$  are the magneto-electric ones<sup>22,23</sup>. We set  $c = \epsilon_0 = \mu_0 = 1$  since they will not be relevant parameters. Finally, the composition symbol denotes convolution in both space, time and the vector indexes.

Since we are interested in characterizing the topology of solely the electromagnetic field, we will set all external sources to zero. For homogeneous materials, we can restate Eqs. (1) and (2) in the Fourier space

$(-i\nabla \rightarrow \mathbf{k}, i\partial/\partial t \rightarrow \omega)$  and reorganize them in a more compact matrixial form:

$$L_{\omega,k} \mathbf{f} = (iR_k + \omega M_{\omega,k}) \cdot \mathbf{f} = 0 \quad (4)$$

$$\mathbf{k} \cdot \mathbf{D} = 0, \quad \mathbf{k} \cdot \mathbf{B} = 0 \quad (5)$$

where  $\mathbf{f} = (\mathbf{E}, \mathbf{H})^T$  and

$$R_k = \begin{pmatrix} 0 & \mathbf{S} \cdot \mathbf{k} \\ -\mathbf{S} \cdot \mathbf{k} & 0 \end{pmatrix} \quad (6)$$

is the  $6 \times 6$  matrix associated to the curl part of the equations and does not depend of  $\omega$ ; here  $(S^i)_{\alpha\beta} = i\epsilon^{i\alpha\beta}$  is formed out of the totally antisymmetric rank 3-tensor and is an element of a spin-1  $SU(2)$  algebra<sup>14,24</sup>. Since at finite frequency the equations in (5) are implied by Eq. (4), they will be omitted in the rest of the paper.

We assume the matrix  $M$  to be Hermitian (lossless material condition) and to be real when expressed in spatial coordinates, hence  $M(\omega, \mathbf{k}) = M^\dagger(\omega, \mathbf{k}) = M^*(-\omega, -\mathbf{k})$ . Moreover, as  $M$  describes causal responses, it is analytical in the upper half complex  $\omega$ -plane. We also take that the residues of  $M$  are semi-positive definite, which guarantees the semi-positiveness of the energy fields. Few important properties follow: the eigenfrequencies  $w_k$  of Eq. (4) are real<sup>25</sup>;  $L_{\omega,k} = -L_{-\omega,-k}^*$ ; each solution  $(w_k, \mathbf{f}_{\omega_k,k})$  at finite frequency pairs up with a solution at opposite energy and momentum  $(-w_k, \mathbf{f}_{-\omega_k,-k}^*)$ . The latter conditions identify a symmetry which we will refer to as particle/hole symmetry throughout the paper.

We are interested in interface modes in (effectively) 2D gyrotropic materials in the  $(x, y)$  plane. Usually there are two ways to define a 2D problem: the first one is to physically confine the fields along the plane with two metallic plates<sup>26</sup>, and the second is to deal with a 3D system but assuming invariance along the transverse  $z$  direction ( $k_z = 0$  in Eq. (4)). For the sake of simplicity, we shall opt for the second one. For the discussion of examples, later we shall consider uniaxial responses of the material concerning the permittivity tensor (gyro-electric effect) or the permeability tensor (gyro-magnetic effect) with  $\hat{z}$  as the principal axis. In these case, the  $6 \times 6$  set of Maxwell equations simplifies into two uncoupled sets of  $3 \times 3$  equations operating on  $(E_x, E_y, H_z)$  and  $(H_x, H_y, E_z)$  that are respectively referred to as transverse magnetic (TM) and transverse electric (TE) modes.

**Topology and bulk-boundary correspondence**—The advantage of using topology is to predict the existence of physically relevant modes by avoiding a direct calculation of the eigenfunctions of Eq. (4) with an inhomogeneous, frequency dependent matrix  $M_{\omega,k}$ .

The basic tool to do so is the vector bundle associated to each band. To define them, we solve Eq. (4), compute the bands dispersion  $w_k^{(i)}$  and the associated eigenvectors  $\mathbf{f}_k^{(i)}$ . Then for each band we can define a fiber bundle, that consists in the collection of the projectors onto the eigenvectors of a band  $P_k = \mathbf{f}_k \mathbf{f}_k^\dagger$  (called fibers)

parametrized by  $(k_x, k_y)$ , elements of  $\mathbb{R}^2$  (called the base space,  $\mathcal{M}$ ).

For a generic fiber bundle we shall consider the scalar quantity for each band:

$$C = \frac{1}{2\pi i} \int_{\mathcal{M}} dc_1 dc_2 \text{Tr} P (\partial_1 P \partial_2 P - \partial_2 P \partial_1 P) \quad (7)$$

where  $c_{1,2}$  are two generic coordinates on the base space and  $\partial_{c_j}$  the associated partial derivative. When  $\mathcal{M}$  is compact,  $C$  has the remarkable property to be an homotopy invariant integer and is called the (first) Chern number. The Chern number can be used to quantify a number of physical effects. In particular, the number of states  $N_{chiral}^\sigma$  localized at interfaces between two materials, whose frequency migrate toward a band  $\sigma$  as the momentum along the interface goes from lower to higher values, is computable via a so-called bulk-boundary correspondence<sup>12,27</sup>:

$$N_{chiral}^\sigma = C_{right}^\sigma - C_{left}^\sigma \quad (8)$$

where  $C_{left/right}$  is the band Chern numbers computed from the bulk response of the left or right material relative to the band  $\sigma$ . Negative values of  $N_{chiral}^\sigma$  mean opposite flow direction.

Eq. (8) can be applied in lattices, such as photonic crystals, where the first Brillouin zone form a compact base space. On the contrary, the formula is not directly applicable in continuum systems like ours, as  $\mathcal{M} = \mathbb{R}^2$  is non-compact. In Ref.<sup>13</sup> it has been shown indeed that  $C$  takes non-integer values for some bands of a gyrotropic material with local dispersion. To define an integer Chern number for a band in continuum problems, further assumptions on the behaviour of  $M$  at large  $|\mathbf{k}|$  are to be made to make the base space  $\mathcal{M}$  effectively compact<sup>13,14,16,18,19</sup>. However, in the large  $|\mathbf{k}|$  limit the small scale structure of the material, being either inhomogeneous or crystalline, comes out. Therefore a microscopic approach beyond the macroscopic Maxwell's equations is demanded, implemented either with field sources ( $\rho$  and  $\mathbf{J}$ ) or Bloch theory respectively<sup>28</sup>. For that reason, we propose to follow a different strategy to predict the existence of interface chiral modes.

**Spectral flow from Berry Monopoles**—The approach we follow essentially consists in describing a continuous interpolation between two media where the "bulk" spectrum closes at some point during the interpolation. The quantized Berry flux emanating from this degeneracy point is a first Chern number that fixes the number of chiral modes trapped at the interface. The advantage of this method is that it does not require that bulk bands of the continuous materials from each side of the interface have a (well-defined) non-zero Chern number. In spirit, this approach is very similar to a 2D version of the celebrated Jackiw-Rebbi model where the mass term in the Dirac equation changes sign along a direction<sup>29,30</sup>. An optical analog of this model, where the

anisotropic mass term is played by an anisotropic Faraday effect, was already derived by Raghu and Haldane in their pioneering paper on topological photonics<sup>25</sup>. However, this model was derived as an effective description in the vicinity of a Dirac point emerging in the full band structure of the photonic honeycomb crystal, so that the topological properties were derived by means of the compact Brillouin zone.

To be definite, suppose that we have two semi-infinite materials in contact along the  $y$ -axis ( $x = 0$ ) and characterized by two different bulk responses  $M_1$  and  $M_2$  respectively. We assume that the interface is defined by a *smooth* change of an extrinsic parameter (e.g. an applied magnetic field) or intrinsic one (e.g. the permittivity tensor). Therefore, the response matrix is described by a space dependent operator  $M(\tau(x), i\partial_x, k_y)$ , where  $x$  is assumed to enter  $M$  via an interpolating smooth function  $\tau(x)$  such that when  $\tau(x) = 1$  (resp.  $-1$ ) then  $M = M_1$  ( $M_2$ ). For instance, the following linear interpolation is one such family (we drop the dependence from  $i\partial_x$  and  $k_y$ ):

$$M(\tau(x)) = \frac{M_1 + M_2}{2} + \tau(x) \frac{M_1 - M_2}{2}, \quad \tau(x) = \tanh(x/x_0) \quad (9)$$

The idea of our approach is to add the spatial coordinate as an independent parameter for an extended base space of fiber bundle. It is cleaner to add  $\tau$  itself rather  $x$ . The new base space is therefore made of terns  $(\tau, k_x, k_y) \in [-1, 1] \times \mathbb{R}^2$ , on which the so-called symbol of the response matrix  $M(\tau, k_x, k_y)$  is defined. To define the fibers, we enforce the computation of the eigenvectors from Eq. (4) treating  $\tau$  and  $k_x$  as independent (commuting) variable. Next, we identify points  $p^{(l)} = (\tau^{(l)}, k_x^{(l)}, k_y^{(l)})$  of band-degeneracy in this extended fiber bundle, i.e. points at which  $\omega^{(i)}|_{p^{(l)}} = \omega^{(j)}|_{p^{(l)}}$ ,  $i$  (resp.  $j$ ) denoting an upper (lower) band. For the sake of simplicity, here we consider only cases where such points are isolated (Berry monopoles). To proceed further we construct small 2-spheres  $\mathcal{S}_l$  that enclose each monopole separately (in the case of line degeneracies we would construct enclosing cylinders<sup>31</sup>). Finally, we consider the fiber bundles having these spheres as base spaces and the eigenvectors of one of the bands involved as fibers (see Fig. 1). Assuming there is a gap shared by the right and left bulk, we claim the following spectral flow formula

$$N_{chiral}^{l,\sigma} = -C^{(l,\sigma)} \quad (10)$$

where  $N_{chiral}^{l,\sigma}$  is the number of localized states in the gap flowing towards the band  $\sigma$  as  $k_y$  goes from lower to higher values than  $k_y^{(l)}$ ;  $C^{(l,\sigma)}$  is the Chern number, as from Eq. (7), with  $\mathcal{M} = \mathcal{S}_l$  and  $P$  projecting on the eigenvectors of the band  $\sigma$ .

The formula has its mathematical roots in the theory of deformation quantization<sup>32-34</sup>. The latter relates spectral flows of one-parameter families of *quantum* operators (for instance the spectral projection over one band) to the

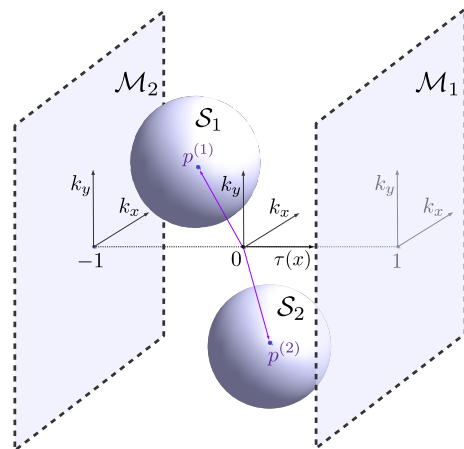


FIG. 1: Extended base space with the bulk base spaces  $\mathcal{M}_{1,2}$  and base spaces  $\mathcal{S}_l$  around generic degeneracy-points (particle hole symmetric point are not shown).

topological index of the associated fiber bundle (e.g. that of the projectors  $P$ ) over the *classical* base space.

Few remarks have to be made: *i*) The minus sign in the formula depends on the orientation of the axis-tern of extended base space. Here we agree with the convention of Refs.<sup>32</sup> and<sup>33</sup>. *ii*) The formula can be extended to the case where more than two bands are involved in the degeneracy. Whenever this is the case, more than one gap have to be considered, and the spectral flows concern only the gaps between (spectrally) adjacent bands. *iii*) There will always be a degeneracy line at  $|\omega| = |\mathbf{k}| = \infty, \forall \tau$  due to the vacuum response limit of  $M$ . However, the projectors  $P$  in that limit are the same for any material. This invariance guarantees that no role is played by this degeneracy. *iv*) When  $\omega^{(l)} = k_y^{(l)} = 0$  and the number of bands involved is odd, particle-hole symmetry enforces the vanishing of  $C^{(l,0)}$  for the central band. For the rest, this symmetry does not imply any constraint in the definition of the complex fiber bundles and does not affect the spectral flow formula, the only implication being that for any degeneracy point at  $(\tau, k_x, k_y)$  in the extended base space there will be a corresponding one at  $(\tau, -k_x, -k_y)$ . *v*) The map from the operator to the symbol,  $M(\tau(x), i\partial_x, k_y) \mapsto M(\tau, k_x, k_y)$ , is not the simple replacement of the first entry in the cases where  $\tau(x)$  and  $i\partial_x$  appears in products<sup>33,35</sup>. However these cases are not investigate in the reminder of the paper. *vi*) The nature of the degeneracy points in the extended base space might depend on the family of matrices  $M(\tau)$  describing the interface. This feature is not present in crystals. There, Chern numbers can be computed in the Brillouin zones  $\mathcal{M}_1$  and  $\mathcal{M}_2$  of the two materials and their difference must equate the total Berry flux emanated by the monopoles across *any* possible homotopy  $M(\tau)$  with  $M(\pm 1)$  kept fixed. This equivalence cannot be stated in the continuum case, instead classes of topologically

equivalent interfaces can be defined. A change of class could be determined by degeneracy points coming from or going to  $|\mathbf{k}| = \infty$  with  $-1 < \tau < 1$ .

**Application to gyrotropic continuous media**– We show now that the spectral flow formula Eq. (10) correctly predicts the number of chiral Maxwell modes for various interfaces between different optical continua. We take under consideration three materials: a perfect electric conductor (a Drude metal with high plasma frequency), a gyro-electric material (a Drude magnetized plasma) and a gyro-magnetic one (ferrite), the last two under a magnetic field  $B_z$  oriented along  $z$ . The first material serves as a "trivial insulator" from the point of view of the topological theory, while the other ones are already known to feature topological physics. The three response matrices are listed in Table I (we neglect non-hermitian lossy contributions)<sup>36</sup>. There,  $\omega_p$  is the plasma frequency of the material,  $\omega_m \propto B_z$ ,  $\omega_b \propto S_z$  ( $S_z$  being the value of the saturated magnetization) and  $\omega_c \propto B_z$  is the cyclotron frequency. Notice that the magnetized plasma response reduces to that of the metal when the magnetic field is switched off. As previously said, the specific form of these responses implies that TE and TM modes are uncoupled. In the following we will focus only on the interesting modes of each case, namely, TE modes for interfaces with ferrite and TM modes for those with magnetized plasma.

Before addressing the interface problem between these different materials, it is instructive to focus on a simple case which is fully analytically solvable. This model is obtained for the magnetized plasma in the regime  $\omega_c \gg \omega_p, \omega$ . According to the permittivity tensor in Table I in that limit, the Maxwell's equations (4) for the TM modes simplify into the explicit eigenfrequency problem

$$\begin{pmatrix} 0 & i\Omega & -k_y \\ -i\Omega & 0 & k_x \\ -k_y & k_x & 0 \end{pmatrix} \begin{pmatrix} E_x \\ E_y \\ H_z \end{pmatrix} = \omega \begin{pmatrix} E_x \\ E_y \\ H_z \end{pmatrix} \quad (11)$$

where  $\Omega = \frac{\omega_p^2}{\omega_c}$ . Note that this electromagnetism model is (up to a rotation  $k_y \rightarrow -k_x$  and  $k_x \rightarrow k_y$ ) formally equivalent to the linearized two-dimensional shallow water model encountered in fluid dynamics, where the electric field plays the role of the in-plane fluid velocity, and where the magnetic field component plays the role of the thickness variation of the fluid. The fluid mechanics analog of the frequency parameter  $\Omega$  is the Coriolis parameter. In the geophysical context, this parameter changes sign at the equator, giving rise to two eastward waves trapped at the equator as found by Matsuno<sup>37</sup>. The topological properties of this model have been unveiled recently<sup>20</sup>. Here, we found its electromagnetic analog. The eigen-frequencies of this model constitute three continuous bands  $\omega_{\pm} = \pm\sqrt{k_x^2 + k_y^2 + \Omega^2}$  and  $\omega_0 = 0$  that touch in parameter space  $(\Omega, k_x, k_y)$  at  $p^{(0)} = (0, 0, 0)$ . As explained in the previous section, a fiber bundle can be constructed from each eigenstate on a sphere that encloses this three-fold degeneracy point in the parameter

space (see figure 1). In the local spherical coordinates, where  $k_x = k \cos \phi$ ,  $k_y = k \sin \phi$  and  $\Omega = \omega_+ \cos \theta$ , the projector on the band of positive frequency reads

$$P_+ = \frac{1}{2} \begin{pmatrix} s_\phi^2 + c_\theta^2 c_\phi^2 & -s_\theta^2 s_\phi c_\phi + ic_\theta & s_\theta(ic_\theta c_\phi - s_\phi) \\ -s_\theta^2 s_\phi c_\phi - ic_\theta & c_\phi^2 + c_\theta^2 s_\phi^2 & s_\theta(ic_\theta s_\phi + c_\theta) \\ s_\theta(-ic_\theta c_\phi - s_\phi) & s_\theta(-ic_\theta s_\phi + c_\phi) & s_\theta^2 \end{pmatrix} \quad (12)$$

where the shorthands  $s$  and  $c$  denote sine and cosine functions. From formula (7), one can finally infer the value of the Chern number for this fiber bundle that is  $C^{(0,+)} = -2$ . This topological property guaranties that two chiral modes reaching the positive frequency band emerge for the dual problem where one considers now a smooth spatial variation of  $\Omega$  along  $x$  that changes sign, as for instance  $\Omega \rightarrow \Omega(x) = \frac{\omega_p^2}{\omega_c} x/x_0$  where  $x_0$  is an arbitrary length that we can choose such that  $x_0 = \omega_c/\omega_p^2$ . The eigenvalue problem becomes

$$\begin{pmatrix} 0 & ix & -k_y \\ -ix & 0 & i\partial_x \\ -k_y & i\partial_x & 0 \end{pmatrix} \begin{pmatrix} E_x \\ E_y \\ H_z \end{pmatrix} = \omega \begin{pmatrix} E_x \\ E_y \\ H_z \end{pmatrix} \quad (13)$$

and can be solved analytically by use of Hermite polynomials. The frequency spectrum is shown in Fig. 2The plots label need to be divided by  $k_0$  and  $\omega_0$ . It shows a spectral flow (dashed lines) in agreement with the topological numbers, where the two, dispersive and non-dispersive, chiral waves have the respective dispersion relations  $\omega = \pm\frac{1}{2}(k_y \pm \sqrt{k_y^2 + 4})$  and  $\omega = k_y$ . These modes are trapped around  $x = 0$  with the following profile along

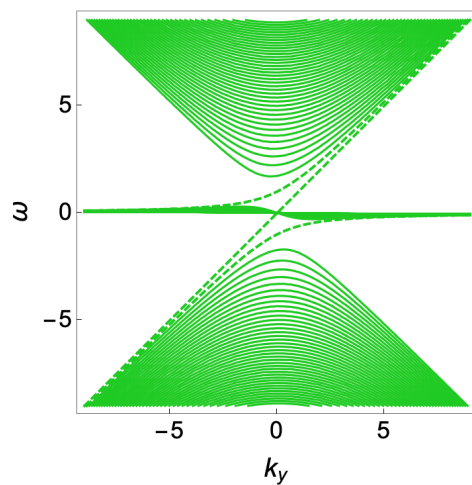


FIG. 2: Dispersion relation of the transverse magnetic modes in a gyro-electric continuum media with  $\Omega(x)$  a linear function of  $x$ .

	Metal	Ferrite	Magnetized plasma
$\epsilon$	$\left(1 - \frac{\omega_p^2}{\omega^2}\right) \mathbb{1}$	$\mathbb{1}$	$\begin{pmatrix} 1 - \frac{\omega_p^2}{\omega^2 - \omega_c^2} & i \frac{\omega_p^2 \omega_c}{\omega(\omega^2 - \omega_c^2)} & 0 \\ -i \frac{\omega_p^2 \omega_c}{\omega(\omega^2 - \omega_c^2)} & 1 - \frac{\omega_p^2}{\omega^2 - \omega_c^2} & 0 \\ 0 & 0 & 1 - \omega_p^2/\omega^2 \end{pmatrix}$
$\mu$	$\mathbb{1}$	$\begin{pmatrix} 1 - \frac{\omega_m \omega_b}{\omega^2 - \omega_m^2} & i \frac{\omega \omega_b}{\omega^2 - \omega_m^2} & 0 \\ -i \frac{\omega \omega_b}{\omega^2 - \omega_m^2} & 1 - \frac{\omega_m \omega_b}{\omega^2 - \omega_m^2} & 0 \\ 0 & 0 & 1 \end{pmatrix}$	$\mathbb{1}$

TABLE I: Dielectric coefficients for the materials under consideration.

the  $x$  direction

$$\begin{pmatrix} E_x \\ E_y \\ H_z \end{pmatrix} = \begin{cases} \begin{pmatrix} e^{-x^2/2} \\ 0 \\ e^{-x^2/2} \end{pmatrix} & \text{non dispersive} \\ \begin{pmatrix} -i \frac{x}{\omega - k_y} e^{-x^2/2} \\ e^{-x^2/2} \\ i \frac{x}{\omega - k_y} e^{-x^2/2} \end{pmatrix} & \text{dispersive} \end{cases} \quad (14)$$

We are now ready to move on to more complex situations by performing numerical simulations of the following interfaces  $M_1/M_2$ : (a) ferrite ( $B_z > 0$ )/ferrite ( $B_z < 0$ ); (b) ferrite/metal; (c) magnetized plasma ( $B_z > 0$ )/magnetized plasma ( $B_z < 0$ ); (d) magnetized plasma/metal. In order to avoid unwanted issues with physical boundaries we have set periodic boundary conditions along the  $x$ -axis i.e.  $\mathbf{f}(x = x_0, k_y) = \mathbf{f}(x = -x_0, k_y)$  ( $x_0$  is set as the unit of length) closing the systems to what would be a cylindrical geometry if we neglect the  $z$ -direction. We interpolated according to Eq. (9) and chose the function  $\tau(x)$  such that one material is in the half-cylinder (in unit  $x_0$ )  $x \in [-0.5, 0.5]$  while the other in  $x \in [-1, -0.5] \cup [0.5, 1]$ :

$$\tau(x) = \tanh[\alpha(|x|/x_0 - 0.5)] \equiv \tanh \xi(x) \quad (15)$$

where  $\alpha$  is a barrier width parameter and  $\xi$  is a rescaled displacement from the barriers. This geometry allows one to simply highlight the opposite propagating direction of the topological modes localized at different interfaces.

In Fig. 3 we show the band dispersions  $\omega(k_y)$  computed numerically<sup>38</sup>. The material parameters for the simulations are written below Fig. 3. The simulation parameters are common to all cases:  $N_x = 240$  (number of point for discretization along  $x$ -axis),  $\alpha = 120$ . We did not aim here to a quantitative description of the physics but to a quantitative one. For each instance we show in Fig. 4 the eigenfrequencies calculated at  $|\mathbf{k}| = 0$  and highlight the degeneracy points in the extended space in going across the interface at  $x = 0.5x_0$ .

In these setups TE and TM modes are decoupled. For the cases (a) and (b) we have shown only the TE modes

while for cases (c) and (d) only the TM ones. Let us comment now on the results in the Figs. 3 and 4 case by case: (a). There is a single pair of (particle/hole symmetric) Berry monopoles sitting at  $(\tau, k_x, k_y) = (0, 0, 0)$  of Chern number  $|C^{(1,\sigma)}| = 2$  with corresponding frequency  $|\omega^{(1)}| \sim 100\omega_0$ . In agreement with Eq. (10), two chiral states (in yellow in Fig. 3) traverse the gap at that frequency. Correspondingly, two states flow in the opposite

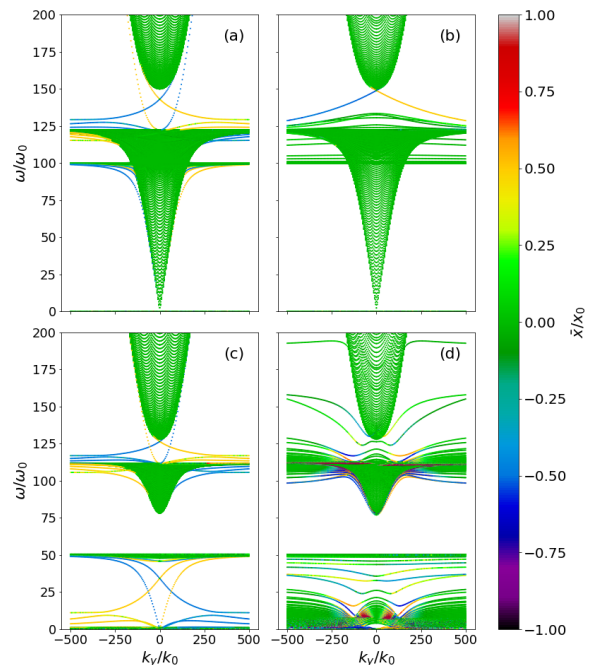


FIG. 3:  $\omega$ -positive band dispersion in a cylindrical geometry for different combinations of materials. Cases (a-d) as in the main text. The colorbar shows the average localization of the eigenstates. Parameters of Table I: (in unit  $\omega_0 = 2\pi c/x_0$ ) for ferrite,  $\omega_b = 50, \omega_m = 100$ ; for magnetized plasma,  $\omega_c = 50, \omega_p = 100$ ; for metal,  $\omega_p = 1000$ .

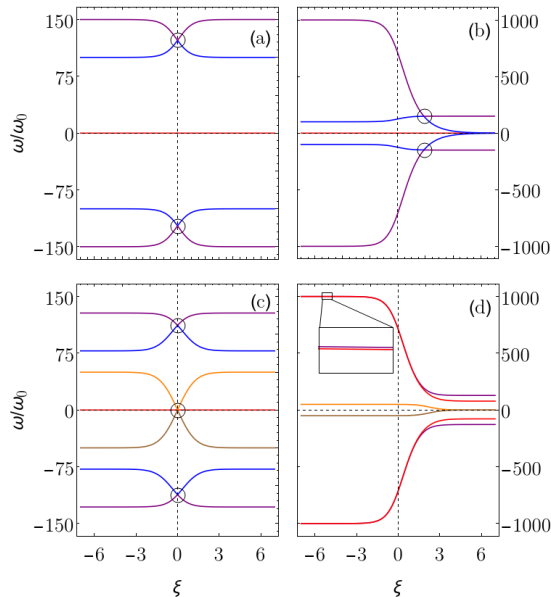


FIG. 4: Local eigenfrequencies at  $|\mathbf{k}| = 0$  as a function of the rescaled displacement from the interface. Berry monopoles are highlighted with circles. Same interfaces and materials parameters of Fig. 3.

direction at the other interfaces. *(b)*. There is still one pair of degeneracy points, however they are shifted at position  $\simeq (\tanh 1.9, 0, 0)$  due to the non-symmetric configuration and  $|C^{(1,\sigma)}| = 1$ . The computation of the Chern number without using Eq. (7) is detailed in Eq. (A1). *(c)* This interface is the most interesting. All monopoles are sitting at  $(0, 0, 0)$ , but they are of different kind. In particular a pair corresponds to  $|\omega^{(1)}| \sim 100\omega_0$  and involves the two uppermost and lowest bands with  $|C^{(1,\sigma)}| = 2$ ; an other single monopole at frequency  $|\omega^{(2)}| = 0$  involves 3 bands with  $C^{(2,\pm)} = \mp 2$  for the upper (lower) band,  $C^{(2,0)} = 0$  for the central one. In agreement with Eq. (10), a pair of chiral states traverses the gap at the frequency  $|\omega^{(1)}|$  and another pair traverses the gap above  $|\omega^{(2)}|$  in the opposite direction. The topological states associated to  $|\omega^{(2)}|$  remarkably do not overlap in frequency with the TE modes, the latter lying at higher frequencies,  $\omega > \omega_p = 100\omega_0$ , as explained in ??). They are therefore good candidate for a clean experimental detection. *(d)* This interface is a critical one as the monopole is present only asymptotically at  $\xi = -\infty$ , which is not attained in the simulation. We found no in-gap topological states. Curiously, states emerge outside the bulk bands. They are evanescent states localized at different interfaces but they are hybridized because of the finite size of the  $x$ -direction. They could be of topological origin<sup>39</sup> but this analysis goes beyond the purpose of the paper.

A careful look at Fig. 4 may reveal an apparent contradiction already mentioned in Ref.<sup>40</sup>. The bulk bands (i.e. at  $|\xi| \gg 1$ ) of a material may look different in the different subfigures. For instance, consider the metal case at

$\xi = -7$  in (b) and (d). In (b) the middle band (in blue) is at  $\omega = 100\omega_0$  while in (d) the corresponding band (in orange) is at  $\omega = 50\omega_0$ . These frequencies stem from the frequency-poles of the respective response matrices, that of the ferrite in (b) and that of the magnetized plasma in (d). However, in the limit of infinite  $|\xi|$  the residues of these poles vanish implying the disappearance of the electromagnetic mode<sup>45</sup>. We conclude that their bulk limit is not physically relevant. As a check, for cases (a) and (c) we have repeated the simulations with a different interpolation, perhaps more physical, assuming  $B_z$  (and therefore  $\omega_{m,b,c}$ ) to be linearly interpolated across the interface. All monopoles are sitting at  $(0, 0, 0)$  with vanishing frequency, we found the sets of Chern numbers to be the same as the cases above. As a consequence the spectral flow is also unchanged. Allowing for  $B$  to rotate in the  $xz$  or  $yz$  planes would allow also to check for the robustness of the spectral flow. However, line degeneracies appears in the extended base space that are left out from the present discussion. We compare our analysis with an interface problem found in literature in Appendix B.

**Conclusion**– We showed how topological chiral modes at smooth interfaces between continuous optical media can be predicted by means of a spectral flow formula, even when the materials involved are not topological. In this context Berry monopoles happen to more "fundamental" than band Chern numbers being the former local, always computable quantities and latter global ones of limited use. Our claims are supported by an analytical low-frequency model for gyro-electric TM modes and a numerical study of interfaces for various well known gyrotropic materials where we predicted the existence of chiral states. This work calls for a number of attractive possible extensions. First, in the paper we have restricted the analysis to spectral flows at vanishing  $k_z$ . Enabling finite values opens up to the full 3D spectrum and we expect Weyl physics to take place. Second, it would be interesting to consider hybrid interfaces between continuous media and photonic crystal or, conversely, interfaces between hybrid materials that are continuous along some dimensions and patterned along the others. Third, linear degeneracies<sup>31</sup> have been left out from our work, however they seem to appear quite naturally in the continuous context. Their inclusion will lead to a more complete version of the spectral flow formula. Finally, we have limited our discussion to the class of materials identified by Raghu and Haldane. To investigate more general responses, for instance bearing losses<sup>41,42</sup> or relative to meta-materials<sup>43,44</sup>, will allow to make contact with more promising and realistic continuous media interfaces in future works.

This work was supported by the French Agence Nationale de la Recherche (ANR) under grant Topo-Dyn (ANR-14-ACHN-0031).

## Appendix A: Calculation of the Chern number

The definition of Chern number Eq. (7) makes use of the Levi-Civita connection. Our formula is equivalent and have to be compared with the one proposed by Raghu and Haldane for optical systems and widely used in literature<sup>25</sup>:

$$C = \frac{1}{2\pi} \int_{\mathcal{M}} dc_1 dc_2 (\partial_1 \mathcal{A}_2 - \partial_2 \mathcal{A}_1) \quad (\text{A1})$$

where the (non-standard) Berry connection is  $\mathcal{A}_j = -\text{Im} \mathbf{f}^\dagger (\partial_\omega \omega M) \partial_j \mathbf{f}$ . Notice that sometimes  $\mathcal{A}_j$  is defined with a minus sign affecting the sign in Eq. (7) as well.

The reason for the equivalence of the two expression is that Chern characteristic classes and therefore the Chern number are independent from the specific connection one uses<sup>32</sup>. A direct consequence is that the polarization modes that contributes to Eq. (A1) through the term  $(\partial_\omega \omega M)$  are actually of no topological relevance. In practical calculation it suffice therefore to integrate  $P$  in the spherical coordinates of  $\mathcal{S}_l$  with a flat connection i.e. with  $(c_1, c_2) = (\theta, \phi)$  and no additional Jacobians in the integrand. To verify the correctness of the results we have also calculated  $C$  by means of a different technique explained in Ref.<sup>33</sup>. We consider the projector  $P$  onto a band and construct  $s = P \mathbf{v}$ , with  $\mathbf{v}$  an arbitrary vector.  $s$  is a global section of the vector bundle on  $\mathcal{M}$  that will vanish generically at some set of points  $\{p_j\}$ . Then we consider the winding of the complex phase of  $z_j = s^\dagger \mathbf{f}_{p_j}$

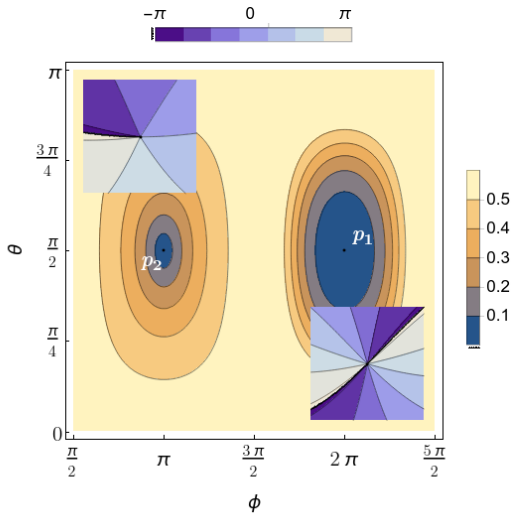


FIG. 5: Norm of the global section  $s$  over the base space  $\mathcal{S}$  parametrized by (shifted) spherical coordinates  $(\theta, \pi)$ . for the uppermost band of the case ferrite/metal. In the inset, the complex phase of  $z_j$  in the vicinity of the vanishing-norm points.

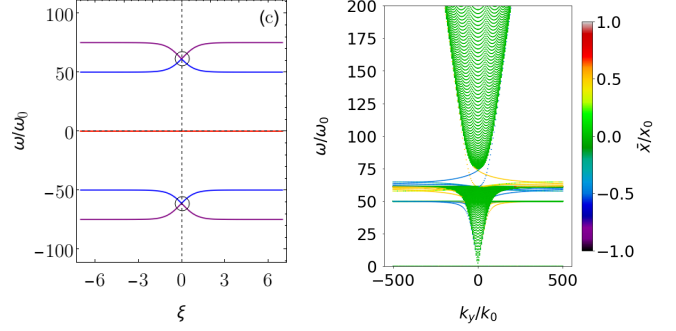


FIG. 6: Topology from Berry monopoles for a the gyrotropic material of Ref.<sup>40</sup>. (left) Local eigenfrequencies as in Fig. 4. (right) Positive-frequency bands in cylindrical geometry. Parameters (in unit  $\omega_0$ ):  $\omega_m = 50$ .  $\omega_b = 25$ .

(remember that  $P = \mathbf{f} \mathbf{f}^\dagger$ ) with  $s$  evaluated along a path that encircle  $p_j$ . One can show that  $C = \sum_j \text{wind}(z_j)$ . We show the numerical technique applied to the case metal/ferrite as in Fig. 4(b). The Berry monopole is at  $\xi \simeq 1.9$  and  $|\mathbf{k}| = 0$ . Therefore we set the base space  $\mathcal{S}$  at the degeneracy point, a sphere with radius  $0.3x_0$  stretched by a factor 1000 along the momenta directions. As one can see in Fig. 5, the global section related to the uppermost band vanishes in two points  $p_1$  and  $p_2$  and their associated winding is, respectively, 2 and  $-1$ . Therefore the total winding is  $1 = C$  as indeed confirmed by applying Eq. (7) to the Fig. 3(b).

## Appendix B: Comparison with Ref.<sup>40</sup>

We apply our approach to a case studied in Ref.<sup>40</sup>. The author considers a gyrotropic material which has the same response matrix as that of ferrite if we would have inverted permittivity and permeability:  $\epsilon = \mu^{ferr}$  and  $\mu = \epsilon^{ferr}$  (cf. Table I). As mention in the main text, in order to compactify the base space a momentum cutoff in front of the gyrotropic part of the response is added such that the off-diagonal terms vanish at big  $\mathbf{k}$ . The spectral flow of a system with a sharp interface between the material with opposite magnetization at opposite sides of the interface is considered. With the cutoff the band Chern numbers are well defined and, using Eq. (8),  $N_{chiral}^+ = 2$  is found for the uppermost band. It is of our interest the situation with no cutoff inserted where the band Chern numbers cannot be computed. The author finds only a single edge states, the missing one being "flown" towards infinite momenta. We have reproduced the result using the parameters of Fig. 8 in the article. For our theory to be applicable we assume a smooth interface. As it can be seen from our Fig. 6, we have a single pair of Berry monopoles of charge  $|C| = 2$  therefore our result agrees

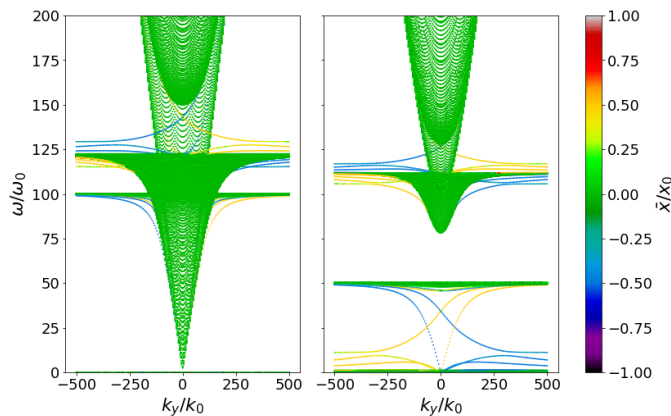


FIG. 7: Band dispersions of cases (a) (in the left) and (c) (in the right) of Fig. 3 in the main text. TE and TM modes are shown together.

with the finding of the reference at finite cutoff. In agreement with our theory we find two chiral states traversing

the gap instead of one as expected for a sharp interface according to the reference.

### Appendix C: TE and TM modes overlapping

As mentioned in the main text TE- and TM-modes bands overlap in the band dispersion. In Fig. 7 we plot again cases (a) and (c) of Fig. 3, showing together both kind of bands. In the ferrite interface the TM modes have the free-light conical dispersion, therefore they span all energies, in particular also the band gap at  $\omega \simeq 140\omega_0$ . Since TE and TM modes are coupled in usual experiments due to impurities or boundary effects, we cannot expect chiral edge states to be easily detected. Fortunately, this inconvenient is not universal. The TE-modes bands dispersion of the magnetized plasma case is actually gapped for  $0 < \omega < \omega_p$  since the dispersion is that of a Drude plasma. As a consequence the spectral flow of the topological chiral TM modes sitting in the lower gap is robust under disorder and boundary effects.

- <sup>1</sup> D. J. Thouless, M. Kohmoto, M. P. Nightingale, and M. den Nijs, *Phys. Rev. Lett.* **49**, 405 (1982).
- <sup>2</sup> M. V. Berry, *Proc. Royal Soc. A.* **392**, 45-57 (1984).
- <sup>3</sup> C. Nayak, S. H. Simon, A. Stern, M. Freedman and S. Das Sarma, *Rev. Mod. Phys.* **80**, 1083-1159 (2008).
- <sup>4</sup> X. L. Qi and S. C. Zhang, *Rev. Mod. Phys.* **83**, 1057-1110 (2011).
- <sup>5</sup> T. Ozawa, H. M. Price, A. Amo, N. Goldman, M. Hafezi, L. Lu, M. Rechtsman, D. Schuster, J. Simon, O. Zilberberg, I. Carusotto, *Rev. Mod. Phys.* **91**, 015006 (2019).
- <sup>6</sup> L. M. Nash, D. Kleckner, A. Read, V. Vitelli, A. M. Turner, and W. T. M. Irvine, *Proc. Natl. Acad. Sci. U. S. A.* **112**, 14495-14500 (2015).
- <sup>7</sup> C. L. Kane, T. C. Lubensky, *Nature Phys.* **10**, 39 (2014).
- <sup>8</sup> S. D. Hüber, *Nature Physics* **12**, 621 (2016).
- <sup>9</sup> Z. Yang, F. Gao, X. Shi, X. Lin, Z. Gao, Y. Chong, and B. Zhang, *Phys. Rev. Lett.* **114**, 114301 (2015).
- <sup>10</sup> X. Zhang, M. Xiao, Y. Cheng, M.-H. Lu, and J. Christensen, *Commun. Phys.* **1**, 97 (2018).
- <sup>11</sup> Z. Wang, Y. Chong, J. D. Joannopoulos and M. Soljačić, *Nature* **461**, 772 (2009).
- <sup>12</sup> E. Prodan, H. Schulz-Baldes, *Bulk and Boundary Invariants for Complex Topological Insulators: From K-Theory to Physics*, (Springer, Switzerland, 2016).
- <sup>13</sup> M. G. Silveirinha, *Phys. Rev. B* **92**, 125153 (2015).
- <sup>14</sup> T. Van Mechelen and Z. Jacob, *Phys. Rev. A* **98**, 023842 (2018).
- <sup>15</sup> M. G. Silveirinha, *Phys. Rev. X* **9**, 011037 (2019).
- <sup>16</sup> A. Souslov, K. Dasbiswas, M. Fruchart, S. Vaikuntanathan, and V. Vitelli, *Phys. Rev. Lett.* **122**, 128001 (2019).
- <sup>17</sup> C. Tauber, P. Delplace, A. Venaille, arXiv:1902.10050 (2019).
- <sup>18</sup> C. Tauber, P. Delplace, A. Venaille, *Journal of Fluid Mechanics*, 868, R2 (2019).
- <sup>19</sup> G. E. Volovik, *Sov. Phys. JETP* **67**, 1804 (1988).
- <sup>20</sup> P. Delplace, J. Marston, and A. Venaille, *Science*, p. eaan8819 (2017).
- <sup>21</sup> M. Perrot and P. Delplace and A. Venaille, *Nat. Phys.* (2019) (in press).
- <sup>22</sup> D. N. Astrov, *Sov. Phys. JETP* **13**, 729 (1961).
- <sup>23</sup> F. R. Prudêncio and M. G. Silveirinha, *Phys. Rev. A* **93**, 043846 (2016).
- <sup>24</sup> K. Y. Bliokh, D. Leykam, M. Lein, F. Nori, *Nature Commun.* **10**, 580 (2019).
- <sup>25</sup> S. Raghu and F. D. M. Haldane, *Phys. Rev. A* **78**, 033834 (2008); F. D. M. Haldane and S. Raghu, *Phys. Rev. Lett.* **100**, 013904 (2008).
- <sup>26</sup> J. D. Jackson, *Classical Electrodynamics* 3rd edition (New York: Wiley) (1999).
- <sup>27</sup> G.M. Graf and M. Porta, *Commun. Math. Phys.* **324**, 851 (2013).
- <sup>28</sup> T. Van Mechelen and Z. Jacob, arXiv:1812.01183 (2018).
- <sup>29</sup> R. Jackiw, *et al.*, *Nucl. Phys. B* **190**, 253-265 (1981).
- <sup>30</sup> J. C. Y. Teo and C. L. Kane, *Phys. Rev. B* **82**, 115120 (2010).
- <sup>31</sup> B. Bradlyn, J. Cano, Z. Wang, M. G. Vergniory, C. Felser, R. J. Cava and B. A. Bernevig, *Science* **353**(6299), aaf5037 (2016).
- <sup>32</sup> B.V. Fedosov, *Deformation quantization and index theory*, (Akademie Verlag, Berlin) (1996).
- <sup>33</sup> F. Faure, arXiv:1901.10592 (2019).
- <sup>34</sup> F. Faure and B. Zhilinskii, *Phys. Rev. Lett.* **85**, 960 (2000).
- <sup>35</sup> M. Zworski, *Semiclassical Analysis (Graduate Studies in Mathematics Series)*, Section 4, (American Mathematical Society, Providence, RI) (2012).
- <sup>36</sup> A. Eroglu, *Wave Propagation and Radiation in Gyrotropic and Anisotropic Media* (Springer Science and Business Media, New York, 2010).
- <sup>37</sup> T. Matsuno, *Journal of the Meteor. Society of Japan. Ser. II* **44**, 25-43 (1966).
- <sup>38</sup> K. J. Burns, G. M. Vasil, J. S. Oishi, D. Lecoanet, B. P.

- Brown and E. Quataert. See the Dedalus entry in the Astrophysical Source Code Library, <http://ascl.net/1603.015>, and the Dedalus project homepage, <http://dedalus-project.org> (2018).
- <sup>39</sup> K. Y. Bliokh, D. Smirnova, F. Nori, *Science* **26**, 1448-1451 (2015).
- <sup>40</sup> M. G. Silveirinha, *Phys. Rev. B* **94**, 205105 (2016).
- <sup>41</sup> M. G. Silveirinha, *Phys. Rev. B* **99**, 125155 (2019).
- <sup>42</sup> B. Zhen, C. W. Hsu, Y. Igarashi, L. Lu, I. Kaminer, A. Pick, S.-L. Chua, J. D. Joannopoulos, and M. Soljacic, *Nature* **525**, 354 (2015).
- <sup>43</sup> G. De Nittis and K. Gomi, *Rev. in Math. Phys.* **31**, 1, 1950003 (2019).
- <sup>44</sup> H. T. Jiang, H. Chen, H. Q. Li, Y. W. Zhang, J. Zi, S.Y. Zhu, *Phys. Rev. E* **69**, 066607 (2004).
- <sup>45</sup> Mathematically, a factor  $\omega - \omega_{pole}$  factorizes out in some lines the Maxwell's equations.